JET–P(99)10

M Tunklev et al

Modelling of Passive Charge Exchange Emission and Neutral Background Density Deduction in JET

JET–P(99)10

Modelling of Passive Charge Exchange Emission and Neutral Background Density Deduction in JET

M Tunklev[1], P Breger[2], K Günther, M von Hellermann, R König[3], M O'Mullane[4], K-D Zastrow.

JET Joint Undertaking, Abingdon, Oxfordshire, OX14 3EA,
[1]Present address: Atomic Spectroscopy, University of Lund, S-223 62, Sweden.
[2]DG-XII/C/5, Rue de la Loi, Wetstraat 200, B-1049, Brussels, Belgium.
[3]MPI für Plasmaphysik, Boltzmannstr. 2, Geb. L7A-123, D-85748 Garching, Germany.
[4]Department of Physics and Applied Physics, University of Strathclyde, 107 Rottenrow, Glasgow, G4 0NG, UK.

Preprint of a Paper to be submitted for publication in
Plasma Physics and Controlled Fusion

April 1999

ABSTRACT.

Passive Charge Exchange (PCX) emission induced by the interaction of neutral deuterium entering the plasma from the walls, and fully ionised light impurities in a tokamak fusion plasma have been investigated. The incentive was to improve the evaluation accuracy of active charge exchange (ACX) spectra, leading to ion temperature, impurity density and plasma rotation. The reconstruction of synthetic line-of-sight-integrated PCX emission spectra is based on a modelled neutral density profile as derived from the FRANTIC code, local emission rates for $D^0(1s)$ and $D^0(2s)$ donor states and finally local impurity ion densities (C^{6+}, He^{2+}) from CX analysis. As a result of the PCX modelling the experimental errors in ion temperature values can be reduced and the range of accessible PCX spectra extended from magnetic axis to separatrix. A comparison between the modelled intensity of the synthetic spectra and experimental PCX data allows also a consistency check of neutral density and its radial distribution.

1. INTRODUCTION TO PASSIVE CX EMISSION

In the plasma core light impurities are fully stripped and may only be detected by the use of active beam Charge Exchange Recombination Spectroscopy (CXRS). Along the Neutral Beam Injection (NBI) path a strong local Active Charge Exchange (ACX) signal can then be detected. It is well known that Passive Charge Exchange (PCX) emission from neutral deuterium in the plasma and the ACX signal, are a composite feature [1-3]. Since the self-consistent deduction of impurity ion density and neutral beam density rely in the first instance on the accuracy of the extracted ACX intensity level, it is of crucial importance to separate the ACX from the PCX. Localisation of the PCX emission layer inside the separatrix has previously been established [4]. This has led to problems encountered in the unambiguous extraction of the PCX feature from the measured spectrum, or more specifically, the problem is that of establishing a true global minimum in the multi-parameter non-linear least square minimisation routine coping with two distinctive regions in the plasma. On the one hand, we consider the plasma core where significant beam attenuation leads to comparable amplitudes of PCX and ACX, but usually with distinctive differences in peak position and width of each spectrum. On the other hand, we consider the outer half of the plasma, where PCX amplitudes are typically less than 5% of the ACX amplitude but have approximately the same peak position and width. In each case it is difficult to establish a global minimum, without initial estimates for each of the free parameters being quite close to the true values. The accurate modelling of the passive emission CX feature is therefore an important step towards the reduction of free parameters or the introduction of constraints for the least-square minimisation process.

The proposed scheme, which is described in this paper, consists of several consecutive steps. In a first approximation, the PCX feature is described by a single Gaussian representing a narrow emission layer close to the separatrix (r/a=0.9). Since for this region the local emission is dominated by the ACX spectrum its Doppler width and shift can also be used as an approximate

description of the PCX, which has much lower amplitude. For the core region, i.e. lines of sight intersecting the neutral beam close to the plasma centre, the ACX results of the edge (r/a=0.9) are then used as initial estimates for both Doppler shift and Doppler-width of the core PCX feature. As will be seen, this is a good initial approximation of the PCX contribution. This procedure and the geometry are described in section 3.

As a result of this first iteration, approximate ion temperatures, ion densities and toroidal rotation profiles can be deduced from the ACX spectra and used as input for the calculation of synthetic PCX spectra. The greatest unknown in this first iteration for the synthetic PCX spectrum is the absolute level of the local neutral density (ground and excited state). The FRANTIC code [5] is used to obtain an initial estimate of the neutral density and its radial distribution. The fraction of excited states $n(D^0,2s)/n(D^0,1s)$ is calculated for the local electron temperature using the photon emissivity coefficient from the ADAS data base [6]. Also, the rate coefficients for CX between D^0(*1s* and *2s*) to C VI (8-7) and to He II (4-3) are taken from ADAS. A comparison of the results of this first approximation (i.e. replacing the true PCX spectrum by a single Gaussian representing an emission layer at r/a=0.9) allows in theory the deduction of local neutral densities. It has therefore been one of the aims of this paper to investigate the scope of neutral density estimates based on a comparison of predicted and observed PCX intensities.

In a second iteration the calculated neutral density profile and a refined synthetic spectrum can be used as input for a further spectral analysis procedure where the PCX shape is kept fixed but its amplitude is optimised. A resulting change of ACX ion temperature, ion densities and rotation can then be used for further iterations

2. CXRS AT JET

The JET CXRS diagnostics uses three 1.3 m, one 1 m, and one 0.75 m, multiple-chord Czerny-Turner spectrometers. Two spectrometers view the plasma vertically sharing two lines of sight, one through the neutral beam in octant 8 for active charge exchange (ACX) between the plasma ions and the energetic neutral beam atoms, and the other one in octant 5 for detection of passive charge exchange (PCX) with neutral background ions in the plasma. These two spectrometers, both equipped with 600 l/mm gratings, are usually set to C VI (*7l -8l'* at 5290.5 Å) and to He II (*3l - 4l'* at 4685.25 Å) with Be IV (*5l - 6l'* at 4659 Å). The other three spectrometers view the plasma horizontally in 12 radial points on the neutral beam injection path from the plasma centre to the plasma edge recording a strong ACX signal, which is Doppler shifted due to the toroidal rotation of the plasma. These spectrometers are set to C VI, Dα (6561.03 Å) and He II / Be IV in order to detect multiple species simultaneously. Neon will be detected as Ne X (*10l - 11l'* at 5249.03 Å) close to the C VI spectrum. These three spectrometers are equipped with gratings of 2160, 2160 and 2400 l/mm respectively, which together with the exit optics, which reduces the image by a factor 4-5, give an effective grating constant of 600 l/mm. Reference lines for wave-

length calibration of each spectrum are for He II / Be IV the Be II transition at 4673.386 Å [7] ($3d\ ^2D$ - $4f\ ^2F$), and for C VI / Ne X another Be II transition at 5270.635 Å [7] ($3p\ ^2P$ - $4s\ ^2S$). These Be II lines emit only at the edge of the plasma outside the Last Closed Flux Surface, and have therefore almost zero Doppler shift even when the confined plasma is strongly rotating. This can be verified since line radiation from a diode pumped Nd:YAG laser at 5321 Å is also imposed into every Carbon spectrum for absolute calibration of the wavelength scale. Data are taken with Peltier-cooled CCD cameras sampling spectra for all the viewing lines every 50 ms as default during the NBI phase, but passive spectra can also be gathered when the NBI is not active. The horizontal spectrometers have in addition to their 12 ACX viewing lines a few lines of sight at the side of the NBI from which horizontal passive emission can be detected. Due to halo effects from beam produced neutral atoms and plume contribution [8], these passive charge exchange measurements tend to be difficult to interpret. Optical fibres guide line radiation from the vessel to the spectrometers behind a concrete wall, which shields from neutron radiation. The optical fibres closest to the torus are heated in order to self-anneal the damage caused by high neutron flux during Tritium experiments [9]. See Fig. 1 for an overview of the CXRS diagnostics.

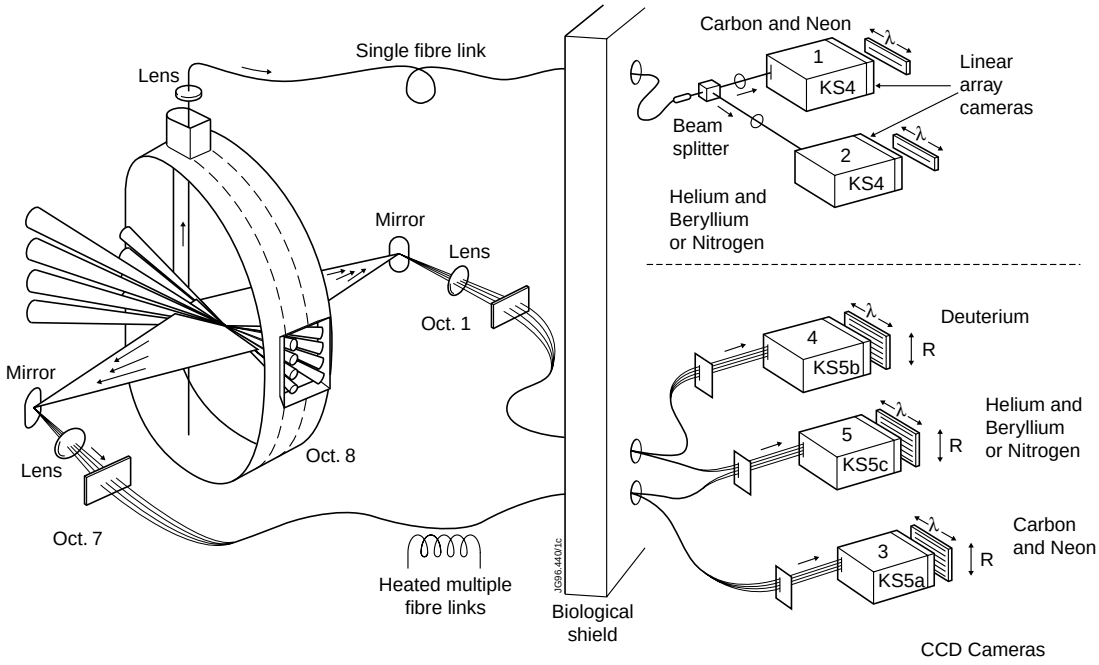

Fig. 1: CXRS Diagnostic system. Spectrometers 1 and 2 are viewing the plasma vertically, and 3,4 and 5 views the plasma horizontally.

The ion temperature and plasma rotation velocity is determined from the Doppler broadening and shift of the deduced ACX components. From these, also the density of the various ions is derived through the intensity of the photon flux. Since the local neutral beam density is determined by the stopping power of the different collisions with electrons, background ions and impurities, an iteration procedure will be used where impurity densities are added succes-

sively thus optimising the NBI density with the various impurity densities for all impurities and background ions. The stopping cross-section for an impurity of charge Z is taken from ADAS and includes the effect of the contributed Z electrons, [6].

3. PROCEDURE OF ANALYSIS

The treatment of the measured spectra implies a very careful analysis in fitting the various ACX Gaussians to their correct spectral components, and an example of this can be seen ahead in Fig. 5. Problems will arise if the identification of the ACX component was uncertain from the very beginning due to blends from either line radiation caused by other impurities, which is reasonably well understood, or line integrated PCX emission from the impurity itself. The latter may very well be the case in both He and C, since these are released from the wall, C as a component of the wall and He from previous clean up Helium glow discharges. Since the gradients of the densities in time and space are essential for a subsequent transport analysis when deriving impurity flux, diffusion coefficients and convection velocities, it is of utmost importance to start the analysis with a well-defined ACX component. The relative intensity of the PCX compared to that of the active component, excited by neutral beam interaction, increases strongly towards the plasma centre when beam attenuation becomes more pronounced and the active signal rapidly diminishes. Representative intensity ratios (passive:active) are of the order 0.05 at the plasma boundary and 1 at plasma centre. For the inner and weaker central channels the least square solution for the fit of active and passive features to the observed sum-spectrum is sometimes ambiguous. For this reason the following model is used to constrain the temperature and velocity of the passive component during the first iteration of the analysis. This model assumes that the spectra from the plasma edge viewing lines (edge l.o.s) are dominated by the active component, and that an additional passive component may be ignored in the analysis. The passive CX component in the composite spectrum representing the plasma centre (centre l.o.s.) may then be linked to temperatures and Doppler shift of the active CX spectrum measured by the edge l.o.s, close to the separatrix, and approximated with a Gaussian. In the least square routine those two values can then be treated as constants and thereby possible uncertainties in the multi-dimensional minimisation of the least-square problem will be reduced. The validity of this procedure will be discussed further in section 4. The Doppler shift is induced by the toroidal rotation of the plasma, and the difference in observation angle α, which is the angle between line of sight and toroidal direction. The wavelength for the PCX emission may then be written:

$$\lambda_{PCX}^{centre} = \lambda_0 + \Delta\lambda_{obs} = \lambda_0 + \lambda_0 \frac{v_{tor}^{edge} \cos\alpha_{l.o.s}^{centre}}{c} = \lambda_0 + \lambda_0 \frac{\Omega_{ACX}^{edge} \cdot R_{impact}^{centre}}{c} \qquad (1)$$

The angular frequency measured at the plasma edge is given by:

$$\Omega_{ACX}^{edge} = \frac{v_{obs}}{R_{edge} \cos\alpha_{edge}} = \frac{(\lambda_{ACX}^{edge} - \lambda_0) \cdot c}{\lambda_0 R_{imp}^{edge}} \qquad (2)$$

which gives:

$$\lambda_{PCX}^{centre} = \lambda_0 + \frac{(\lambda_{ACX}^{edge} - \lambda_0) \cdot R_{imp}^{centre}}{R_{imp}^{edge}} \tag{3}$$

Since it is impossible to separate the PCX from the ACX for the outer regions of the plasma due to their almost complete overlap in wavelength this procedure has only been performed in the region of $\rho \leq 0.5$, with $\rho = r/a$.

4. SIMULATION OF THE PCX COMPONENT

Figure 2 shows the torus from above with the centre and edge viewing lines passing through the plasma. R_{imp} is the minimum distance from the viewing line to the torus centre, and R_{max} is the distance between the viewing port to the torus centre. Each viewing line can be classified with its angle β between R_{max} and the viewing line. The photon flux $\Phi(\lambda,\beta)$ can be expressed as twice the integral over the path of the viewing line in major radius R from the position of R_{imp} at the centre of the viewing line to the wall at the viewing port.

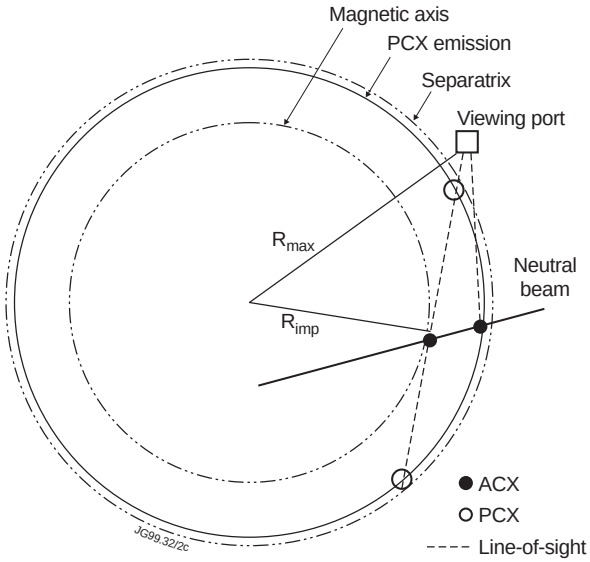

Fig.2: Toroidal view of the plasma from above with the centre and edge viewing lines crossing the NBI path.

$$\Phi(\lambda,\beta) = 2\int_{Rimp}^{Rmax} I_S(\lambda,\beta,R)\varepsilon_{PCX}\frac{RdR}{(R^2 - R_{imp}^2(\beta))^{1/2}} \tag{4}$$

$I_S(\lambda,\beta,R)$ is the Gaussian spectral line profile of the emission, Eq. 7, which is a function of R since the plasma rotation and ion temperature giving the Doppler width are expressed in R, and ε_{PCX} is the estimated local PCX emissivity in R. This can be written:

$$\varepsilon_{PCX}(R) = (4\pi)^{-1} n_0(R) n_i(R) Q(R) \tag{5}$$

with n_0 being the neutral density given from the FRANTIC code, n_i the CXRS measured impurity density, e.g. C^{6+} or He^{2+} , and Q the total effective emission rate as in Eq. 6.

$$Q_{PCX} = <\sigma_{PCX} v_{i,j}> \tag{6}$$

where Q data for CX with Deuterium in states $n=1$ and $n=2$ are taken from ADAS [6], see Fig. A1 and A2 in Appendix A. The importance of including both ground state and excited state hydrogen as donor has been investigated in [10]. The existing cross-sections were valid for a mono-energetic donor acting on a thermal population and have therefore been modified using

the code ADAS313, which converts the data to thermal-thermal charge exchange, see appendix A. The spectral line contribution can be written:

$$I_S(\lambda,\beta,R) = \frac{1}{\Delta\lambda(\pi)^{1/2}} exp\left[-\left(\frac{\lambda-\lambda_0\left(1+R_{imp}(\beta)v(R)/Rc\right)}{\Delta\lambda(R)}\right)^2\right] \quad (7)$$

where c is the velocity of light, $\Delta\lambda$ is the *1/e* half width due to the Doppler broadening. Equation 4 is then solved numerically and the result $\Phi(\lambda,\beta)$ can be seen in Figs. 3 and 4. The absolute value of the neutral density needed to estimate the PCX contribution in the plasma is not well known. However, the radial shape of this profile is reasonably well understood [5, 11, 12], and can be calculated using the FRANTIC code [5], which calculates the neutral population in a cylindrical geometry taking charge exchange recombination processes into account. FRANTIC at JET includes the following main implementations:

- JET geometry in one dimension.
- NBI source of fast and thermal neutrals deposited in the bulk plasma.
- Use of experimental JET data such as edge D_α emission for calculations on the influx of neutrals (when taking molecular fractions into account), measured CX impurity densities and ion temperatures.

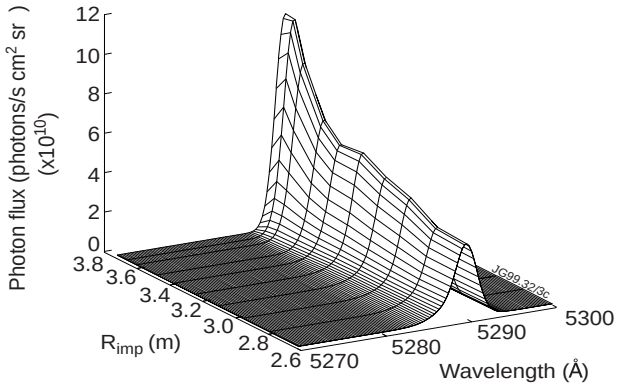

Fig.3: Line integrated PCX signal for Carbon, pulse 43723, t=21s, $T_i \leq 3$keV.

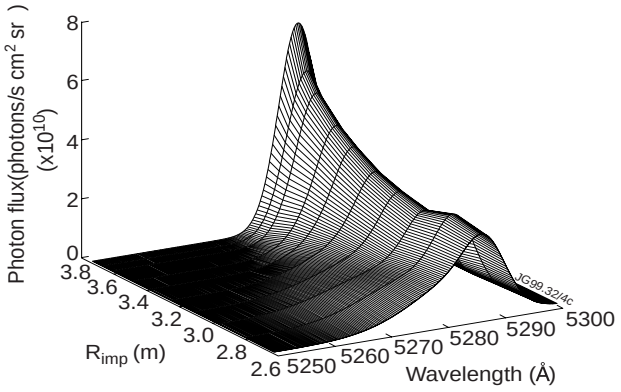

Fig.4: Same as in Fig. 3 but for the maximum DT fusion power JET pulse 42976 with $T_i \leq 34$keV.

However, the code does not take several other general facts into account since the calculation is based on poloidal and toroidal symmetry in a cylindrical plasma, and therefore averaged over the flux surfaces. The main cases not included are:

- Poloidal asymmetries in the D_α emission arising from Hydrogen atoms travelling up to the horizontal mid plane from the divertor.
- The poloidally elongated shape of the plasma.
- The NBI source is averaged toroidally, and the values of the neutral deposition around the CX viewing lines are therefore underestimated, since these are close to the injection path of the NBI.

These points may only be properly modelled in a complete 3D Monte Carlo simulation, but as shown in Figs. 6-9, the need for this is not immediate, since excellent agreement with experimental data is achieved.

The effect of the line integration will be a PCX component containing contributions from every point along the viewing line and therefore not necessarily a Gaussian. In order to reveal the effects of the line integration three different high power shots have been used as an example; the maximised fusion power pulse #42976 ($T_i \leq 34$keV, $\Omega \leq 2.1 \bullet 10^5$rad/s) in ELM free H-mode with hollow Carbon and flat Helium density profiles, #40572 ($T_i \leq 28$keV, $\Omega \leq 2.4 \bullet 10^5$rad/s) in optimised shear, with peaked Carbon density profile, and the low temperature ELMy H-mode discharge #43723 with $T_i \leq$ 3keV. Shot data are given in Appendix B.

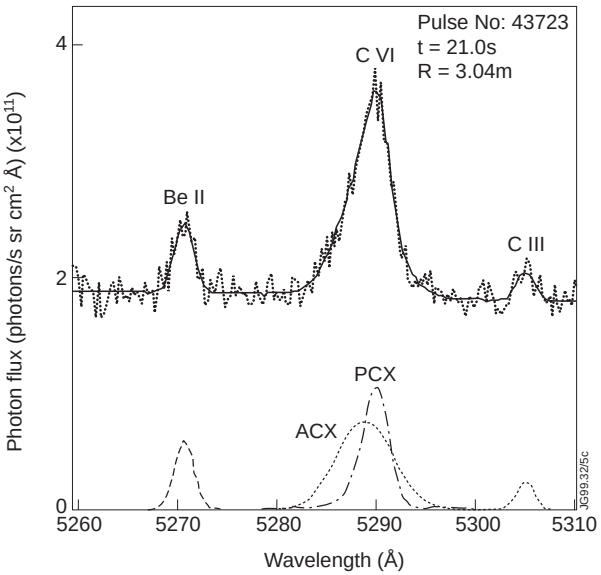

Fig.5: PCX component from Fig. 3, # 43723, with its intensity fitted into the Carbon spectra.

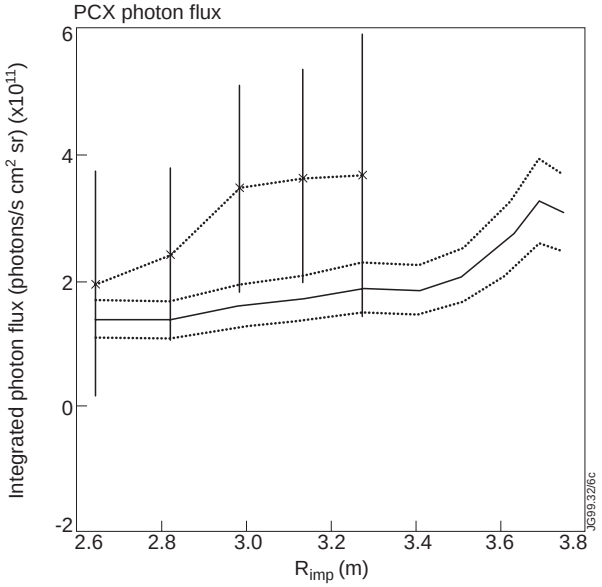

Fig.6: Wavelength integrated total signal for Carbon PCX emission (full)in the various viewing lines denoted with their ACX radii, #43723. Dotted lines are the upper and lower error bars due to errors in the initial values of ion density, temperature, rotation velocity and cross-sections. The neutral density error is set to zero. The experimental measurements using the initial method from equation 5 are given for the inner viewing lines with their corresponding error bars from the least squares fit to the spectra.

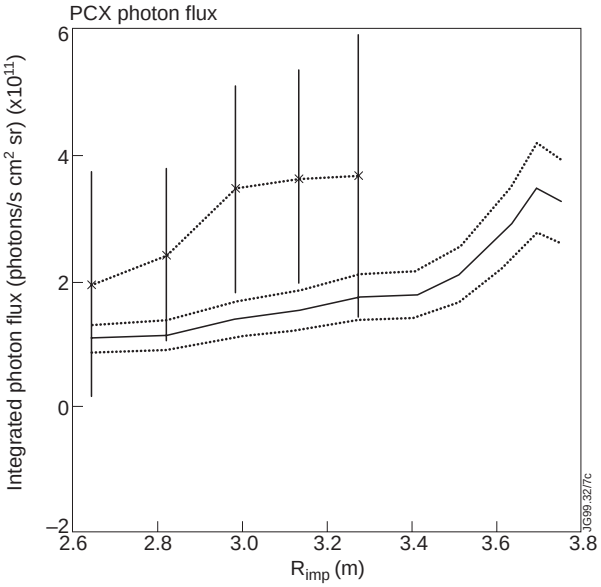

Fig.7: Same as Fig. 6, but for a FRANTIC run with no NBI.

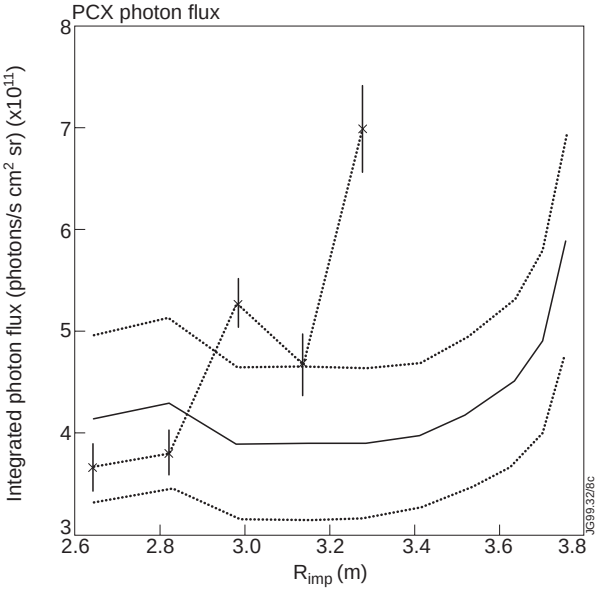

Fig.8: Same as Fig. 6, but for shot 42976.

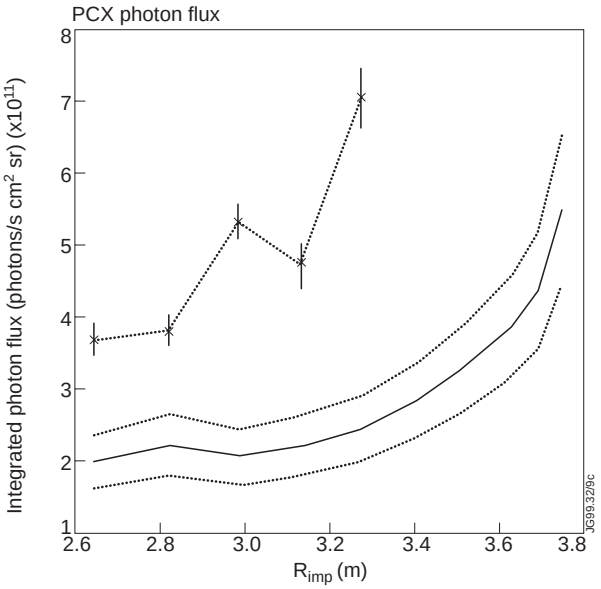

Fig.9: #42976 for a FRANTIC run with no NBI.

As a second iteration in the analysis the synthetic PCX component is now fitted with a non-linear least squares fit to the previously analysed measured spectrum having only its intensity left as a free parameter, Fig. 5. The wavelength integrated photon flux from the first and the second iteration can be seen in Fig. 6, where their agreement shows that the results of the two models used are very close to each other and that the analysis is converging to a consistent result. It is also clearly seen that the synthetic spectra allow a PCX intensity prediction for the outer half of the plasma radius, which is not possible to achieve in the first iteration, due to the complete wavelength overlap. The importance of including the NBI as a donor of neutrals in its surroundings along the CX viewing lines is essential in the analysis of the passive component, especially for hotter plasmas since CX from *n=1* donors is strongly temperature dependent, as seen in Fig. A1 appendix A.

It is seen in Figs. 10-12 that emission from fast rotating hot ions further inside the plasma core is contributing to the signal at the lower wavelengths. This effect can be seen since the effective emission rate from CX with $D^0(n=1)$ donors strongly increases with the plasma temperature, whilst the $D^0(n=2)$ donor rate decreases with the temperature for $T_i \geq$ 7keV. In a plasma with $T_i \geq$ 20keV and impurity density peaked on the toroidal axis two well separated PCX emission layers may be evident since the two different donors are acting at different plasma radii, one at the edge from $D^0(n=2)$ and one further inside from $D^0(n=1)$,

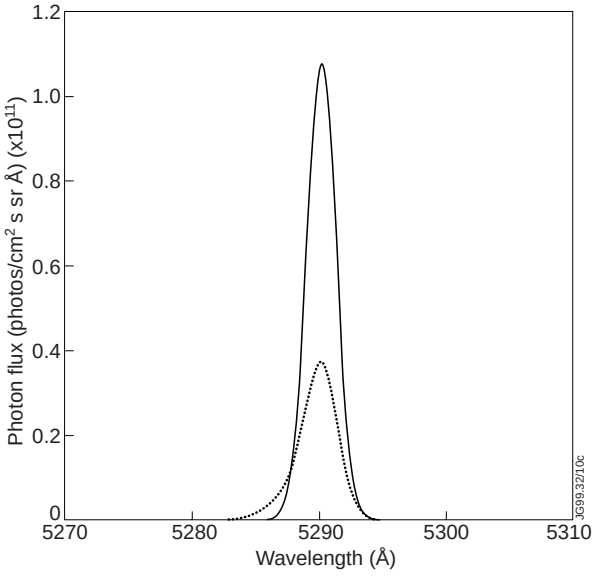

Fig.10: The PCX signal for Carbon #43723, t=21s, centre (broken) and edge (solid).

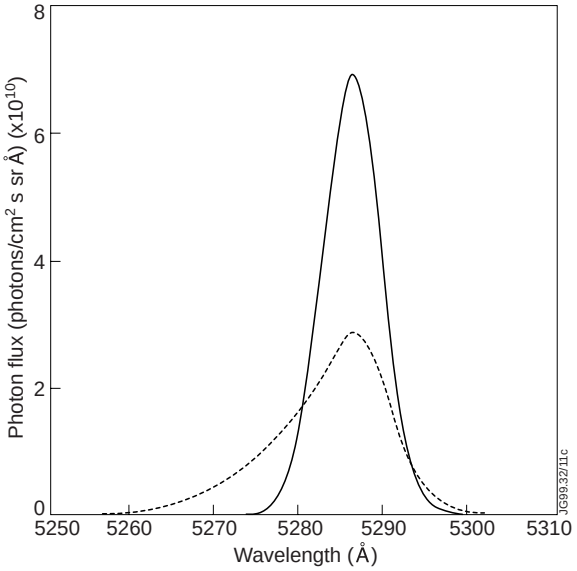

Fig.11: The PCX signal for Carbon #42976, t=13s, centre (broken) and edge (solid). If interpreted as a Gaussian the half width and peak position of the edge component would correspond to an ion temperature of 5.3keV, found at ρ=0.87±0.02, and a rotation of 6•10⁴ rad/s at ρ=0.90±0.02. Using the ACX Doppler shift at 0.90 and equation 5 the wavelength of the centre PCX will be 5287.7Å, which agrees with the peak value of the line integrated signal in the centre viewing line.

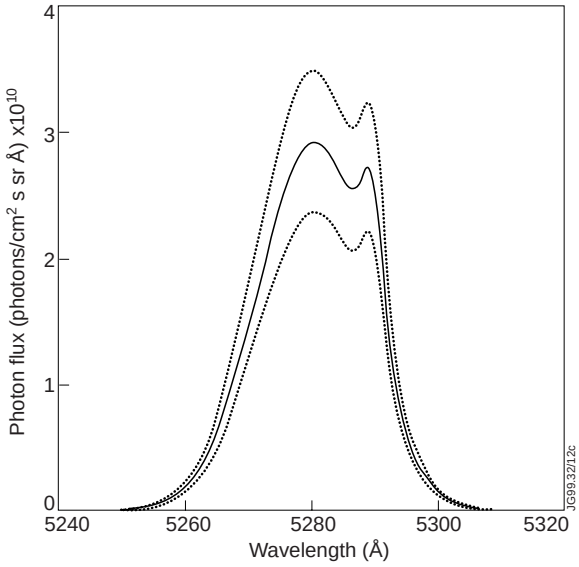

Fig.12: PCX signal for Carbon, #40572, t=6.5s, centre viewing line with R_{imp}*=2.64m. Dotted lines are upper and lower errors as described in figure caption 6. Ion density is peaked on axis and* $T_i \leq 31$*keV with toroidal rotation* $\Omega \geq 2.4 \cdot 10^5$ *rad/s. The contribution from* D^0 *in state n=1 further inside the plasma core is clearly evident at lower wavelengths.*

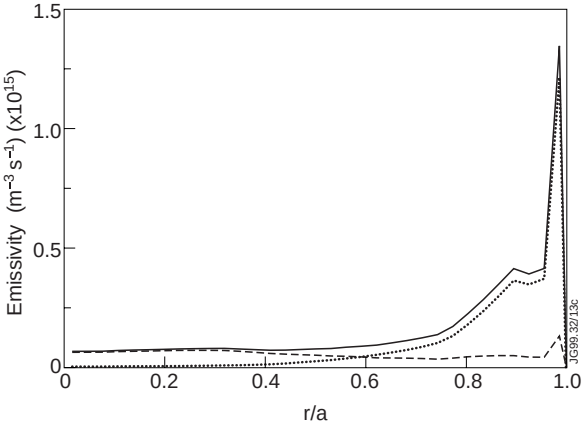

Fig.13: PCX emissivity, #42976, t=13s. The two emission layers arise from CX with D^0*(1s), dashed, and* D^0*(2s), dotted, full line is the sum PCX. (Hollow Carbon density profile).*

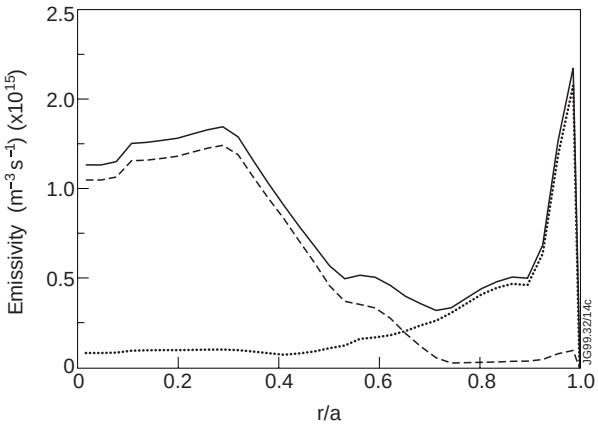

Fig.14: PCX emissivity, #40572, t=6.5s. This is a very clear case of two emission layers, since the Carbon density profile is peaked on axis and $T_i \leq 31$*keV.*

as shown in Figs. 13 and 14. Experimental verification of this prediction is difficult to achieve since the inner emission layer is often totally blended by the ACX, nevertheless it has been seen in several shots that 2 PCX components were needed in order to fit the spectra, one cold at the edge and one hotter from further in. This effect can be ignored for shots with $T_i \leq$ 5keV. However, it has also been found that the spectra of the PCX emission may very well be approxi-

mated with a gaussian for hollow impurity density profiles or plasmas with $T_i \leq 5$keV and $\Omega \leq 1.7 \cdot 10^5$rad/s in the centre. Generally, it has been observed that in cases where the maximum emission from the passive component for peaked impurity density profiles is based in a region with steep gradients in temperature and rotation velocity, it may no longer be advisable to approximate the emission shape with a gaussian profile.

From a analysis of the synthetic PCX spectra based on 12 different plasmas (peaked, hollow, L-mode and H-mode) the improvements in the initial iteration procedure can be summarised as: If the ACX values of width and peak position at $\rho=0.90\pm0.05$ are used to predict the PCX emission in the centre viewing line, the main error will be made in those cases where a strong second emission layer from CX with D(*1s*) atoms exists, in which case the Gaussian approach is less valid. These cases would all be high temperature ($T_i \geq 10$keV) H-mode shots preferably with impurity density peaked on axis. It is also seen that the wavelength of the PCX peak position decreases when looking towards the centre, which is due to the increasing angle between the viewing line and the plasma rotation.

When fitting the synthetic PCX emission into the real spectra it has been found that the signal for both Carbon and Helium is mainly determined by the neutral density at $0.5 \leq \rho \leq 1.0$, whilst Helium shows a relatively higher dependence at $\rho \leq 0.5$ than Carbon. This is mainly due to the different density profiles of the two impurities, since He is usually flat or peaked whilst C is generally hollow. The cross-sections can contribute to this effect due to the following. As seen from Fig. A1 and A2 in appendix A, the value of Q for CX between $D^0(1s)$ with He or C is generally 2-4 orders of magnitude lower than CX with $D^0(2s)$ for 200 eV $\leq T_i \leq$ 35 keV. On the other hand, the population of $D^0(1s)$ is about three orders of magnitude higher than that of $D^0(2s)$, which then makes the two different reactions equally important. The effective Q is best illustrated by using a Q which is weighted with the D^0 populations as Eq 8.

$$\langle Q \rangle = \frac{Q_1 n_1 + Q_2 n_2}{n_{tot}} \tag{8}$$

where n denotes the neutral deuterium density in states 1,2 and total. When T_i increases the fraction of n_2/n_1 will decrease so that $\langle Q \rangle_C / \langle Q \rangle_{He} \rightarrow Q_{1C}/Q_{1He}$, which over the plasma radii will be 1-1.5 for a shot like 42976. Hence, for shots with much lower T_i the effect of Q_2 will be more prominent with a relatively higher population of D^0(2s), and the fraction of $\langle Q \rangle_C / \langle Q \rangle_{He}$ may then be between 3-5, as in shot 43723. When studying the ratio of $\langle Q \rangle_{centre} / \langle Q \rangle_{edge}$ for Helium and Carbon one finds that in shots with lower T_i Carbon does have a higher edge dependence than Helium, whilst for shots with higher T_i they show the same relation. This implies that the somewhat greater sensitivity for Carbon, compared to Helium, on the neutral density at the edge is not only due to its density profile, but also a cross-section effect at lower T_i.

5. CONTRIBUTION FROM RADIATIVE RECOMBINATION

In cold plasmas with T_i less than a few keV and electron densities of about 10^{19} m^{-3}, it will be of interest to investigate whether line emission from electron recombination with free electrons (ER) followed by photon emission, might blend the PCX signal, see relation 9.

$$A^{q+} + e^- \Rightarrow A^{*(q-1)+} \Rightarrow A^{(q-1)+} + h\nu \tag{9}$$

This signal can almost completely overlap the PCX signal in wavelength since the emission arises from the plasma ions at all radii because of the usually flat n_e profile at JET. Figure 15 shows the effective emission rate Q_{ER} for this process for both Helium and Carbon as a function of the electron temperature. Data are taken from ADAS, where level population (*l*-mixing), transition probabilities, dielectronic collision excitation as well as dielectronic recombination are taken into account. This may then be compared to the effective emission rates for the PCX from Figs. A1 and A2 in appendix A. One should bear in mind that even though the values in Fig. 15 are a factor of 10^8 lower than those from Figs A1 and A2, the density of electrons are a factor of 10^7 higher than the neutrals in the plasma centre and the signal may therefore be of importance. Figure 16 shows the emissivity given by Eq. 10, and Figs. 17 and 18 shows the line integrated synthetic spectra.

$$\varepsilon_{ER}(R) = (4\pi)^{-1} n_e(R) n_i(R) Q_{ER}(R) \tag{10}$$

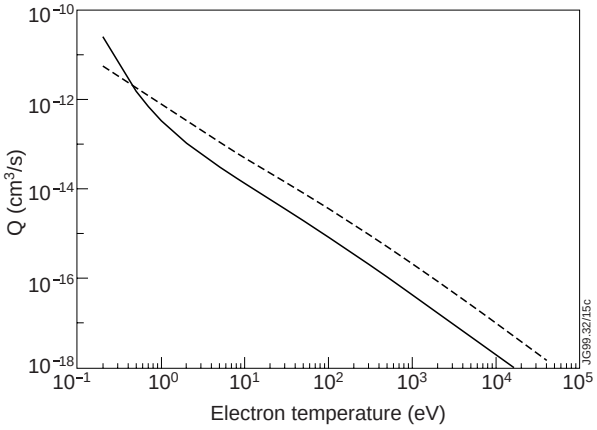

Fig.15: Effective emission rate Q_{ER}, for He^{2+} + $e \rightarrow He^{1+}$ + hν(4685.25Å) (solid) and C^{6+} + $e \rightarrow C^{5+}$ + hν(5290.5Å) (dotted) as a function of electron temperature.

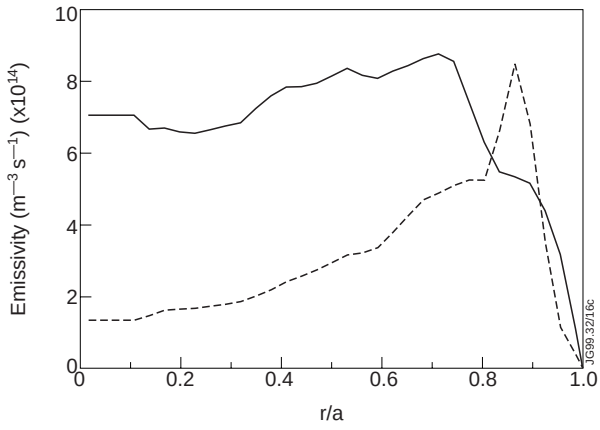

Fig.16: Emissivity of the 4-3 transition in He II (solid) and C VI (dotted) due to electron recombination, #43723, t=21s.

It is seen from comparing Fig. 18 with Fig. 5, that in a plasma like #43723 with T_i<3 keV, the contribution of ER for Carbon can be about 25% of the ACX in the centre l.o.s. Since the ACX is generally 5-10 times more intense at the edge, the effect will be negligible for these viewing lines. In theory the same result holds for Helium, but since the He PCX can be blended by the plume signal [8], an experimental result is more difficult to establish. For shots like 42976 with T_i<34 keV only a very small effect is expected, e.g. ER part of total signal was found to be between 10^{-2} and 10^{-3} times lower than the ACX component for both Helium and Carbon.

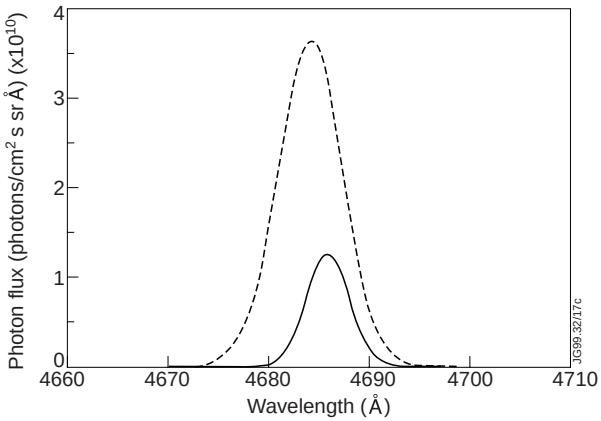

Fig.17: Line integrated spectra of He from the centre (dotted) and edge (solid) l.o.s, #43723,t = 21s. The reversed Doppler shift about 4685.25Å is there since the edge and centre are viewed from different octants opposite the plasma rotation.

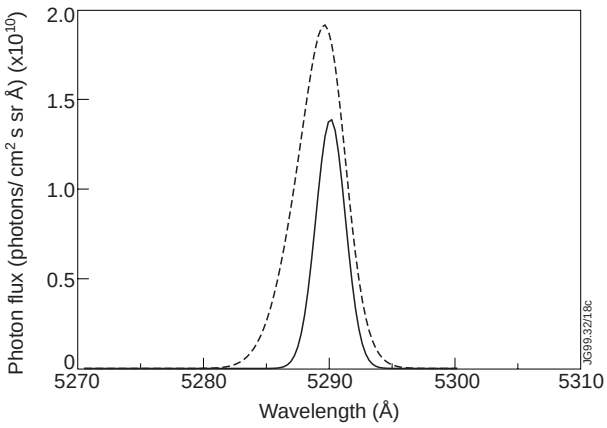

Fig.18: Same as Fig. 17, but for Carbon

6. PCX AND ER MEASUREMENT

For shot 45724 NBI was on in octant 4 and a short NBI blip (500ms) was introduced in octant 8 at 21.5s. This allowed ACX measurements to be performed, and assuming that these results were the same immediately before the beam blip, a PCX calculation can be done using the derived neutral density from 21.4s. The ER emission was included, since $T_i \leq 3$keV, and turned out to contribute 20% to the total model of the synthetic spectra. The sum spectra of PCX and ER were then fitted to the detected spectra at time 21.4 s, see Fig 19. The peak value of the predicted intensity was $1.2 \cdot 10^{11}$ photons/cm^2 s sr Å, which agrees perfectly well with the result from the least squares fit of the spectra.

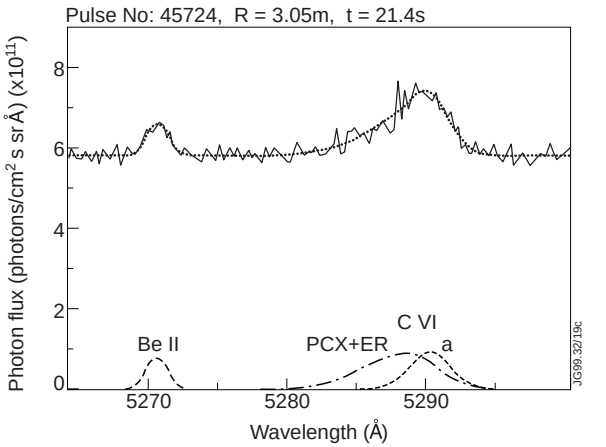

Fig.19: Predicted line integrated synthetic spectra of PCX + ER contributions fitted into a real experimentally detected spectrum, including the electron collision excitation component a.

7. DEDUCTIONS OF NEUTRAL BACKGROUND DENSITY

In most cases this method of treating the PCX component may be used further to establish a more accurate deduction of the neutral background density. Results are shown for pulses 43723 and 42976 in Figs. 20, and 21.

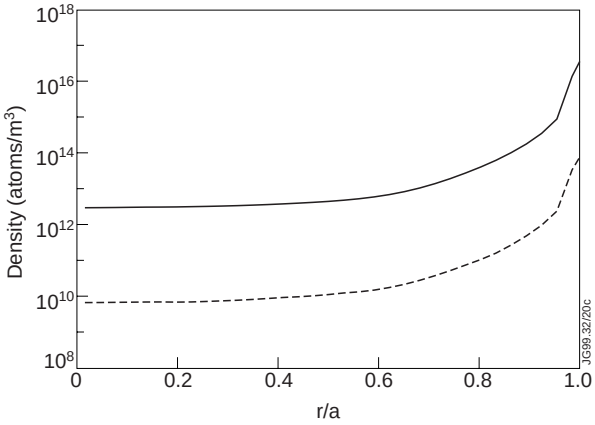

Fig.20: Deduced Neutral Density (H^0+D^0) for pulse 43723, t=21s. The dotted line represents atoms in state 2s *and the solid line in* 1s.

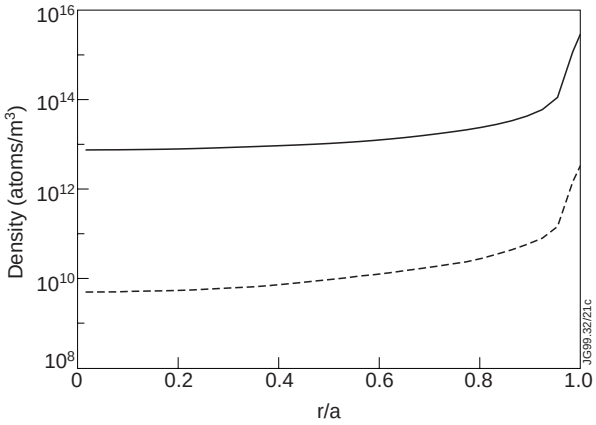

Fig.21: Deduced Neutral Density (H^0+D^0+T^0) for pulse 42976, t=13.0s. The dotted line represents atoms in state 2s *and the solid line in* 1s.

8. CONCLUSIONS

This investigation shows that the modelling of a synthetic PCX spectrum, leads to an improved analysis of the composite C VI and He II CX spectra in hot fusion plasmas. In many cases when $T_i \leq 10$ keV the synthetic spectrum can at first be adequately approximated by a single Gaussian whose peak position and width correspond to the active CX feature measured at $\rho = 0.90 \pm 0.05$. When using a centre viewing line, the FWHM of the PCX emission may increase by 20% and the peak position can be predicted with Eq. 3 to an accuracy of 0.2 Å. However, in the case of steep plasma edge gradients and high pedestal ion temperatures, deviations from a pure Gaussian are clear and a synthetic PCX spectrum will lead to more accurate results.

Moreover, as a result of the PCX modelling and its radial intensity profile, the evaluation range of experimental PCX data may be extended to the very plasma edge. Since the model gives an estimate of the relative intensity expected at the edge, one may fit the centre first, where the PCX is more evident and thereafter fix the edge PCX photon flux according to Fig. 6. This will bring down the ACX photon flux by 5-20% and therefore also decrease, for example in the case of C^{6+} profiles, the degree of hollowness in the deduced density profile.

The PCX measurements from both He II and C VI allow, at least in principle, the deduction of the absolute neutral density value. However, since the main contribution of PCX emission comes from a region close to the plasma edge, only for that region can the neutral densities be sensibly extracted. It is estimated that the uncertainty in cross-sections, which is about 30%, is the main error source. In contrast, our study has shown that the modelled PCX intensity is rather insensitive to variations of the neutral density in the plasma centre, unless $T_i \geq 20$keV and the impurity density is flat or peaked on axis. In these latter cases a second emission layer must be introduced since CX from thermal $D^0(1s)$ atoms is strongly temperature dependent.

The absolute values of the neutral densities derived from the FRANTIC code were confirmed indirectly with the experimental PCX data. The implementation of NBI in FRANTIC as

a donor of thermal and fast neutrals in the vicinity of the CXRS viewing lines, was shown to be efficient as a last step in bringing experiment and theory into agreement.

ACKNOWLEDGEMENTS

Many thanks to Dr. Afanassiev, Ioffe Physical-Technical Institute, St Petersburg for valuable discussions regarding the radial profile of the neutral background density. This work has been supported by the Swedish Natural Science Research Council (NFR).

REFERENCES

[1] A. Boileau, M.G. von Hellermann, L.D. Horton, J. Spence and H.P. Summers Plasma Phys. Controll. Fusion **31**, 779 (1989).

[2] M. von Hellermann and H.P Summers, JET-P(93)34

[3] M. von Hellermann and H.P. Summers, "Atomic and Plasma Material Interaction Processes in Controlled Thermonuclear Fusion", Ed. R. Janev and H.W. Drawin, Elsevier Science Publishers, 135 (1993)

[4] P. Breger et al. 22nd EPS Conference on Plasma Physics and Controlled Fusion, Bournemouth, Contributed papers II, 377 (1995).

[5] S.Tamor, J.of Computational Physics **40,** 104 (1981).

[6] ADAS Atomic Data and Analysis Structure, H.P. Summers et al. University of Strathclyde.

[7] L. Johansson, Arkiv Fysik **20**, 489 (1961).

[8] U.Gerstel, L.Horton, H.P.Summers, M. von Hellermann, B. Wolle Plasma Phys. Control. Fusion **39**, 737 (1997)

[9] A. T. Ramsey, W. Tighe, J. Bartolick and P.D. Morgan, Rev. Sci. Instrum. **68**, 632 (1997)

[10] R Hoekstra et al., Plasma Phys. Controll. Fusion **40,** 1541 (1998).

[11] Y.N. Dnestrovskij, S.E. Lysenko, A.I. Kislyakov, Nuclear Fusion **19**, 293 (1979)

[12] Y.N. Dnestrovskii, D.P. Kostomarov, Numerical Simulation of Plasmas, Springer-Verlag, 200 (1985)

APPENDIX A

Effective Emission Rates for Thermal-Thermal Charge Exchange.

As mentioned in section 4 the emission rates for a mono energetic donor to a thermal acceptor have been modified with the code ADAS313 to account for CX between thermal donor and thermal acceptor. Also, *l*-mixing has been taken into account as well as most CX processes which give rise to photon emission at the specific wavelengths of interest. The results are seen in Figs. A1 and A2.

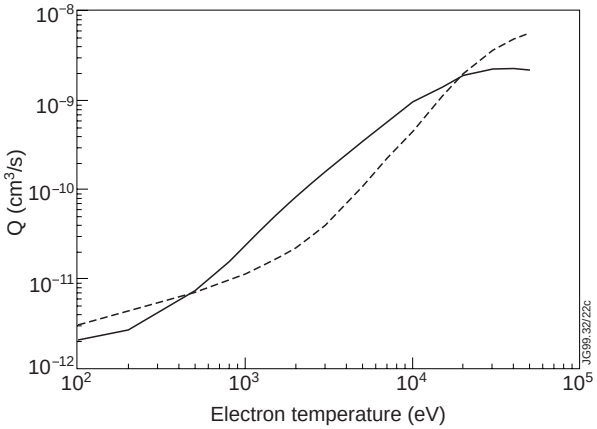

Fig.A1: CX from D^0(1s) to Carbon producing photon emission 5290.5Å *(dotted), and to Helium producing photon emission at* 4685.24Å *(solid).*

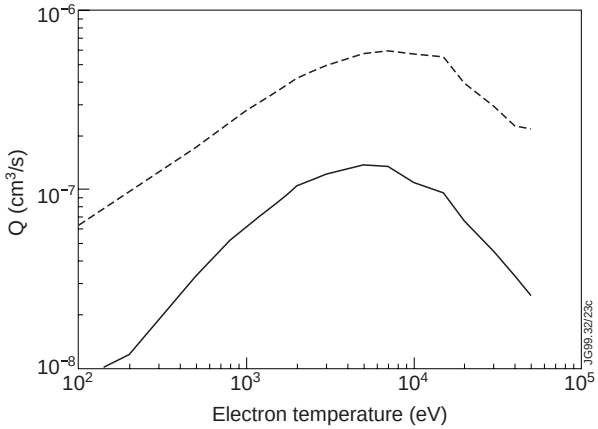

Fig.A2: Same as A1 but with CX from D^0(2s)

APPENDIX B

Shot data: